InSAR Ground Motion Mapping in Support of Urban Resilience and Regional Landscape Planning

Ivana Hlaváčová
dept. of remote sensing
GISAT s.r.o.
Prague, Czechia
ivana.hlavacova@gisat.cz

Jan Kolomazník
dept. of remote sensing
GISAT s.r.o.
Prague, Czechia
jan.kolomaznik@gisat.cz

Juraj Struhár
dept. of remote sensing
GISAT s.r.o.
Prague, Czechia
juraj.struhar@gisat.cz

Erika Orlitová
dept. of remote sensing
GISAT s.r.o.
Prague, Czechia
erika.orlitova@gisat.cz

***Abstract*—CURE project addressed the multidimensionality of urban resilience. The project's App06 component demonstrated the utility of InSAR technology in supporting the assessment of geotechnical hazards in urban or post-mining environments. Results were obtained for two different areas and hazards with a potentially similar impact mechanism on exposed assets – buildings. Geotechnical risks were assessed for assets in Arkalochori, Crete, impacted by a displacement inflicted by the 2021 earthquake, and in Ostrava-Karvina post-mining landscape subjected to gradual ground displacements resulting from mining activity.**

Keywords—InSAR, urban subsidence, urban resilience

I. Introduction

Combined information from Copernicus Core Services has been used in the CURE project to address the multidimensionality of urban resilience. The objective of one of the CURE cross-cutting applications - App06 - was the development and demonstration of InSAR technology supporting the assessment of geotechnical hazards in urban or post-mining environments. The service combined products of different Copernicus Core Services with additional third-party global, national or regional datasets.

A. Geographic context

The Ostrava-Karvina mining area ("POHO landscape ") in Czechia has been subject to long-term ground subsidence impacts resulting from black coal mining activities in recent decades. Furthermore, the gradual attenuation of mining activities and closing of mines lead to variable spatial and temporal distribution sinking hot spots and the emergence of new zones subjected to increased geotechnical hazard due to tensile (hogging) and compression (sagging) strains, respectively. These zones overlap with urban land and existing brownfields. Therefore, investments in the transformation of brownfields need to consider geotechnical hazards to existing and planned buildings related to differential ground deformations at various scales.

The Archalochori earthquake with magnitude 6.0 struck Crete island on Sep 27, 2021, directly causing 1 fatality, 36 injuries and damage to more than 5,000 old buildings [1]. In addition, it initiated a co-seismic ground displacement detectable in both vertical and horizontal directions.

B. InSAR ground motion mapping

Satellite InSAR (Interferometric SAR, Synthetic Aperture Radar) is a method developed in the last 30 years (e.g. [2,3]) for displacement monitoring. Differential InSAR (DInSAR) is the oldest method which uses a pair of SAR images to estimate the displacement between their acquisition. The precision of this method is in the order of centimetres and is suitable especially for isolated events, such as earthquakes.

PSInSAR (Persistent Scatterers InSAR) uses larger stacks (at least 20-30 images) of satellite SAR data to measure long-term displacements (usually more than 1 year). It is suitable for monitoring long-term displacements, which are expected to be linear in time. The precision depends on the number of images, length of the monitoring period etc. and can reach even less than 1 mm/y for displacement velocity, while the precision of one measurement is in the order of mm.

InSAR measures the projection of the 3D displacement to its line of sight (LOS). Therefore, to estimate the displacement direction, i.e. reconstruct the movement, measurements from more satellite tracks with different LOS directions (East vs West) are required [4]. Reliable estimation of the North-South displacement component is not possible from SAR satellite systems operated in the last decade as their side-looking geometries from similar (polar) orbits are insensitive to movements in this direction.

InSAR measurements complement traditional geodetic or geotechnical monitoring techniques and bring several advantages in operational use scenarios dealt with by the CURE pilot. Especially Sentinel-1 imagery, thanks to the availability of the archive since the end of 2014 and continuous measurements, is helpful for:

- Synoptic coverage of a large area of interest (e.g. area affected by an earthquake or mining-related subsidence) and derivation of surface displacement geotechnical hazard indicators
- Retrospective assessment of slow ground displacement evolution in Up and East-West directions
- Ability to assess one-off co-seismic displacements by comparing imagery taken before and after the event

C. Hazard exposure from InSAR

Damage level on buildings and infrastructure caused by subsidence depends on the asset's position in the subsidence bowl, displacement direction and magnitude [4]. Damages such as cracks are typically caused by differential displacements affecting the objects unevenly [5]. In the sinking bowls, the highest hazard is typically concentrated in zones of directional displacement gradients [6].

Recently, several authors developed methodologies allowing the assessment of subsidence-related impacts on vulnerable buildings by using InSAR. [6] detects zones affected by sagging and hogging, differential subsidence rates and angular distortions using Sentinel-1 for larger urban block units. [5] correlates damage severity with subsidence relate intensity described by differential settlements and relative rotation detected for individual buildings using measurements from very-high resolution SAR imagery. The [7] proposes several building-level subsidence classification indexes

considering PSInSAR points from ENVISAT ASAR and their distribution for building polygons. [8] assessed damage probability to vulnerable buildings by assessment of PSI results from both Sentinel-1 and Cosmo-SkyMed SAR imagery.

D. CURE App06

The CURE App06 component aimed at demonstrating the practical utility of combining ground motion from Sentinel-1 with exposure datasets in regional landscape planning or urban resilience domains. Quantifying displacement velocities and their temporal, spatial and direction characteristics allows the assessment of current or forecast future subsidence impacts on exposed assets. The App06 automatically integrates point-wise ground motion measurements into footprints of existing (or planned) assets and zones by their spatial aggregation and derivation of relevant InSAR-based geotechnical proxy indicators to quantify hazards for polygons of exposed assets. The service has been designed to combine datasets from Copernicus Land Monitoring Services (CLMS) - namely: European Ground Motion Service (EGMS) [9] and Urban Atlas land cover land use (UA) [10]. The service is planned to become operational after publishing EGMS datasets via API. For the time being, the demonstration pilot for POHO landscape has been based on the ground motion map originating from own InSAR processing of Sentinel-1 imagery.

TABLE I. COPERNICUS CORE DATASETS

CLMS Dataset	Product level	Spatial representation	Utility
EGMS[a]	L2A, L3: 2015-2020	InSAR measurements (L2: points, L3: 100x100m point grid)	Subsidence hazard
Urban Atlas	Status 2018, Change 2012-2018	Land use building blocks (polygons)	Exposed assets

[a] Not published at the time of CURE implementation (2021). Replaced by proprietary PSI results

II. MATERIALS AND METHODS

A. Datasets

European Ground Motion Service (EGMS) [9] has been providing access to a pan-European continental ground motion map since mid-2022 in the viewer and since October to the archive. The service will provide updates of motion rates on an annual basis which is sufficient frequency for many time noncritical applications. As of version 2018, Copernicus Urban Atlas [10] provides a very-high resolution land cover land use map and change map for 785 functional urban areas across Europe. Without a published EGMS dataset during the CURE project implementation timeline, the subsidence hazards were derived using proprietary InSAR algorithms applied to Sentinel-1 imagery in the POHO area. For Arkalochori, the ground motion was obtained by differential interferometry (DInSAR) based on pairs of Sentinel-1 scenes acquired before and after the event.

TABLE II. SAR IMAGERY

Imagery	Area of interest	
	Arkalochori	*Ostrava-Karvina (POHO)*
Sensor	Sentinel-1 IW, SLC	Sentinel-1, IW, SLC
Tracks	29 (ascending, IW1) 36 (descending, IW3) 102 (ascending, IW1) 109 (descending, IW1)	175 (ascending, IW1) 51 (descending, IW3) 124 (descending, IW1
Period	T29: Sep 24, Sep 30, 2021 T36: Sep 25, Oct 1, 2021 T102: Sep 23, Sep 29, 2021	Oct 2014 – May 2021
Acq. frequency	6 days	6 – 12 days
Total scenes	4 interferometric pairs	300+
InSAR processing [b]	DInSAR (©SARProZ algorithm, track combination)	Multi-temporal InSAR (©SARProZ PSI algorithm, proprietary post-proc enhancements)

[b] By Gisat in the frame of the CURE project

Additional third-party datasets represented a baseline for exposure mapping at a higher level of detail or enhancement of thematic attribution of exposed assets (i.e. providing information about the evolution of urban building blocks).

TABLE III. 3RD PARTY DATASETS

Dataset	Source	Spatial representation	AOI	Utility
WSF-Evol	DLR	Thematic raster	CZ, GR	Exposure Built-up evolution
SRTM30	USGS	Raster DEM	CZ, GR	InSAR topography contribution removal
RUIAN	ČUZK	Polygons (building footprints)	CZ	Exposed assets
Parcels inventory	FORT	Polygons (parcel footprints)	GR	Exposed assets

B. Retrospective MT-InSAR mapping of long-term displacement on Ostrava-Karvina post-mining region, Czech Republic

Ground motion for the POHO area was derived by PSInSAR (Persistent Scatterers InSAR) method implemented in the SARproZ(c) software, and it was demanded to be processed with the best coverage possible. Therefore, all pixels were processed in the POHO area without regard to their amplitude stability. Consequently, many pixels are expected to be noisy due to, e.g. vegetation. The extent of the processed area was extended out of the POHO to allow the selection of a geologically stable reference point. The POHO area is covered by 1 ascending, and 2 descending Sentinel-1 tracks. All the scenes available from the period of October 2014 - May 2021 were initially processed. Due to strong estimated atmospheric variability, less than 10% had to be excluded from processing. Reference points for all satellite tracks were chosen in the stable area out of the POHO.

A long-time series with more than 300 Sentinel-1 images per track brings in higher results accuracy and the possibility of long-time monitoring with dense temporal sampling. On the other hand, it brings challenges for standard PSInSAR algorithms. For example, some points may “disappear” (i.e. get incoherent) during the monitoring period; other points may “emerge“, and both cases may repeatedly occur over the monitoring period. The probability of nonlinear movement is higher over an extended monitoring period, decreasing the overall temporal coherence. Therefore, coherence thresholding, conventionally used to distinguish quality points from low-quality ones, does not give reasonable results, as coherence is “averaged” over the whole monitoring period.

Often, coherence drops under the given threshold due to the time series's nonlinearity or higher noise for part of the monitoring period. Though, such points are the most important for the client.

In addition, phase unwrapping errors emerge if nonlinear displacements are present (displacement velocities at measurement points ranging from several mm/y to several cm/y during the monitoring period). This effect is more pronounced when a periodogram method is used to estimate displacement velocity and when each point is processed independently. Due to strong nonlinearities likely related to the mining activities and phasing-out timeline, unwrapping errors are frequent across measurement points and in a time series of individual points in the POHO area. Unwrapping errors are present in our results and EGMS L2 (Calibrated) product published in mid-2022. Therefore, a proprietary unwrapping error correction algorithm was applied to enhance the processing outputs. The algorithm is based on the segmentation of the long-time series. Some unwrapping errors were not recognized/corrected by the algorithm, and in some cases, the ambiguities cannot be identified even by an experienced InSAR expert. In addition, the correction of an unwrapping error causes a further drop in temporal coherence.After the unwrapping error correction, the time series was split into a couple of segments, and noise (i.e. coherence) was evaluated for each of them individually. The segments are different for each measurement point and should correspond to the displacement history. The quality (i.e. noise level) of each point is then evaluated with regard to this model, and points with inferior quality within a given time period were filtered out before interpretation and further processing.

The L2A output represents the displacement in the LOS direction. To estimate the displacement in vertical and East-West direction (L3 product), the standard decomposition was performed [11] for the POHO area using regular grid cells. The vertical and East-West displacements were calculated only for cells where at least one point from the two descending tracks and at least one point from the ascending track was present. The time series were decomposed only for the period when a sufficient number of points have appropriate quality. All decomposed time series were related to a reference date set to 1.1.2020.

C. *DInSAR mapping of Arkalochori earthquake co-seismic motion*

The earthquake area is well covered by 2 ascending and 2 descending tracks from Sentinel-1. The last pre-event and the first post-event images were acquired and processed from each track. The temporal baseline between the scenes was 6 days in all cases, which allowed for maximizing the interferogram coherence.

Spatial phase unwrapping had to be applied because the LOS displacement was significantly higher than 28 mm (half of Sentinel-1 SAR wavelength). As a result, the atmospheric delay could not be estimated and subtracted for single interferograms. Track 109 had to be discarded due to prevailing unwrapping errors.

Removal of atmospheric delay using 3 pre-earthquake images and 3 post-earthquake images was tested by generating 9 interferograms for each track (with longer temporal baselines) and averaging them. The test proved the interferograms with longer temporal baselines were strongly affected by low coherence leading to phase unwrapping errors that could not be corrected after averaging. Therefore, only one interferogram (per track) without removing atmospheric delay was used as a baseline for subsequent steps.

After an approximate assessment of the earthquake-affected area, interferograms acquired from all tracks were referenced to the phase average of the rest of the processed area, not expected to move.

In the last processing step, displacement maps were spatially filtered and interpolated in order to fill in holes caused by incoherence; the earthquake displacements are expected to have a long-wave effect. Nearest-neighbour interpolation was used as it gave the best results, followed by Gaussian blurring on the whole interferogram. Subsequently, the vertical and East-West components of the displacement were estimated from the (referenced) line-of-sight displacements measured in different tracks. Due to the discarding of track 109, the estimation was implemented from two ascending tracks and one remaining descending track: the one with the flatter incidence angle. This asymmetry may impact the precision of results but not the results themselves. Furthermore, the North-South component was neglected due to the low sensitivity of the Sentinel-1 SAR instrument to this direction. In the case of real movement in the l North-South direction, the vertical component would be biased by about 20% of the real North-South displacement.

D. *Aggregation and geotechnical hazard calculation*

In the long term, strains resulting from displacements often inflict additional damage on buildings. Potential damage severity was evaluated using 2 recent methodologies depending on the spatial analytical unit:

1) For buildings or built-up parcels using the framework introduced by [5]. Potential damage risk is here considered for different classes of building construction materials for building objects. It is proxied by subsidence-related intensity derived from differential subsidence and relative rotation determined by MT-InSAR within the object polygon or its close vicinity. Ancillary metrics (length, width, buffer) were calculated from the polygonal geometry.

2) For larger spatial units such as building blocks or regular grid cells, we came out from the findings of [6]. The methodology assumes differential displacement causing angular distortion and associated strains in vertical and horizontal directions. Subsequently, the tensile (hogging) and compression (sagging) strains were aggregated into a compound indicator: surface faulting hazard. Differential variables were calculated using MT-InSAR product after directional decomposition from radar geometry to Vertical and E-W directions from neighbouring analytical units within a 100m grid for each grid cell.

Variables used for calculations were integrated into targeted analytical units by spatial overlay between the InSAR measurement points and respective polygons. Aggregated variables were derived by zonal statistics. The workflow was automated using Python, Jupyter Notebooks and Docker.

III. RESULTS

A. *Arkalochori*

Results from differential interferometry show a co-seismic displacement that affected the Arkalochori area and surrounding countryside. Displacement maxima detected in the vertical direction exceeded -20 cm. Eastward and

westward displacements were in a lower range, not exceeding +/-10 cm. Measured displacements and their spatial patterns visually correspond to outcomes from other authors [1].

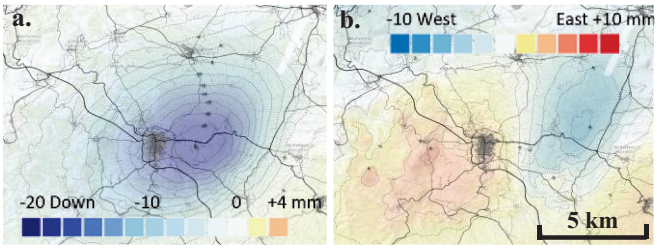

Fig. 1. a. Vertical displacement b. Horizontal displacement in Arkalachori

Associated surface faulting hazard was calculated using specified methodologies.

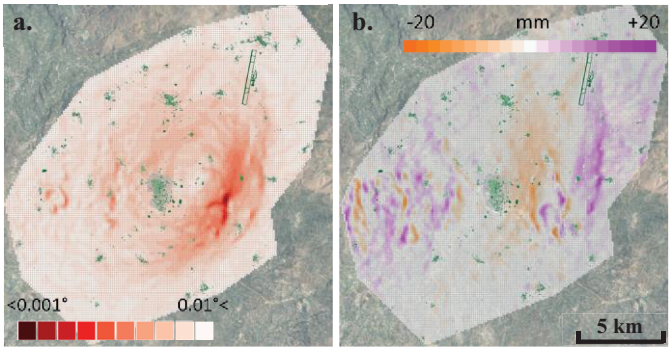

Fig. 2. a. Deflection slope angle b. Horizontal strain

Figure 2a shows a vertical component of the surface faulting hazard derived from the deflection slope angle. The Maxima of the detected slope angle have been below the threshold (0.019°), denoting the boundary between the Low and Medium hazard classes. Consequently, a surface faulting hazard can be categorized as Low in the area. 2b displays the horizontal component of surface faulting hazard referring to horizontal strain. The maxima of horizontal strain indicating sagging and hogging zones remained narrowly below the threshold (0.03 % ~ differential E-W displacement 3 cm) between Low-Medium hazard classes. The deflection slope was then derived as a proxy for potential building damage severity. Estimated maximum values are well below the threshold (0.03°), denoting the boundary between Negligible and Low hazard classes. Therefore, the potential hazard level is classified as Negligible for the area of interest according to [5]. Due to spatial filtering and interpolation, potential local maxima could have been filtered out, leading to underestimating the respective hazard gradient.

B. Ostrava-Karvina region

The distribution of persistent scatterers and measured displacements constituted the estimation of horizontal and vertical strain patterns and associated hazard levels. Hazard zones were provided for multiple development zones planned to be implemented in the POHO post-mining area. Figure 3 shows results in the former Lazy mine.

ACKNOWLEDGEMENT

CURE project has received funding from the European Union's Horizon 2020 research and innovation programme under grant agreement No 870337. The CURE project team was led by Foundation for Research and Technology Hellas (FORTH), Greece. More information can be found at http://cure-copernicus.eu.

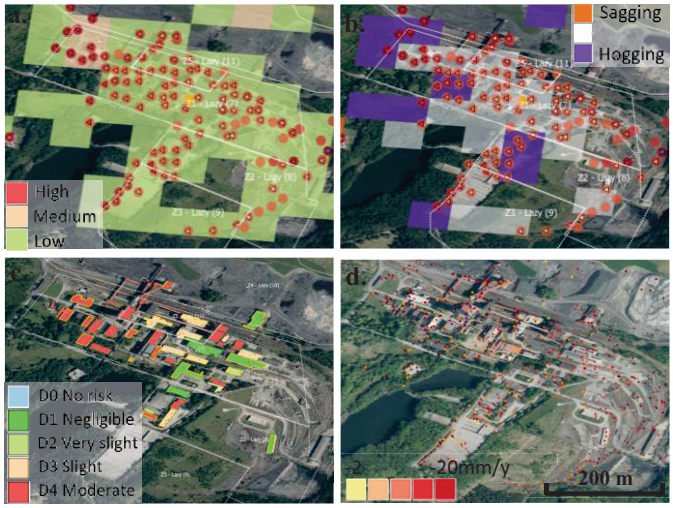

Fig. 3. Hazard zones (after [6]): a. Deflection b. Horizontal strain c. Hazard based on relative rotation for concrete buildings (after [5]) d. Measurement points with LOS displacement velocity. Lazy mine, Ostrava-Karvina POHO

REFERENCES

[1] Triantafyllou I, Karavias A, Koukouvelas I, Papadopoulos GA, Parcharidis I. 2022. "The Crete Isl. (Greece) Mw6.0 Earthquake of 27 September 2021: Expecting the Unexpected" GeoHazards 3, no. 1: 106-124.

[2] Massonnet, D., Feigl, K., Rossi, M. et al., 1994. Radar interferometric mapping of deformation in the year after the Landers earthquake. Nature 369, 227–230 (1994).

[3] Ferretti, A., C. Prati, and Rocca F., 2001. Permanent Scatterers in SAR Interferometry. IEEE Transactions on Geoscience and Remote Sensing 39 (1): 8–20

[4] Saeidi, Ali et al. 2009. Development of building vulnerability functions in subsidence regions from empirical methods." Engineering Structures 31 (2009): 2275-2286.

[5] N. Nappo, D. Peduto, M. Polcari, F. Livio, M.F. Ferrario, V. Comerci,S. Stramondo, A.M. Michetti, 2021. Subsidence in Como historic centre (northern Italy): Assessment of building vulnerability combining hydrogeological and stratigraphic features, Cosmo-SkyMed InSAR and damage data, International Journal of Disaster Risk.

[6] Cigna, F., Tapete, D., 2021. Present-day land subsidence rates, surface faulting hazard and risk in Mexico City with 2014–2020 Sentinel-1 IW InSAR. Remote Sens. of.environ. 253, 1–19..

[7] Garcia, A. J., B. González-Rodrigo, S. Martinez, R. Martinez, and M. Marchamalo. 2021. "Building Health Monitoring in the old Town of Madrid: Applicability of SAR Imagery to the Monitoring of Underground Works Through Classification Indexes." International Journal of Digital Earth 14 (3): 271–287.

[8] Ezquerro, P., M. Del Soldato, L. Solari, R. Tomás, F. Raspini, M. Ceccatelli, J. A. Fernández-Merodo, N. Casagli, and G. Herrera, 2020. "Vulnerability Assessment of Buildings due to Land Subsidence Using InSAR Data in the Ancient Historical City of Pistoia (Italy)." Sensors 20 (10): 2749.

[9] M. Costantini et al. 2021. European Ground Motion Service (EGMS), 2021 IEEE International Geoscience and Remote Sensing Symposium IGARSS.

[10] Copernicus Programme, 2020. Mapping Guide v6.1 for an European Urban Atlas. https://land.copernicus.eu/user-corner/technical-library/urban_atlas_2012_2018_mapping_guide_v6-1.pdf. Accessed Nov 01 2022.

[11] Ketelaar, V.B.H. 2009. Satellite Radar Interferometry: Subsidence Monitoring Techniques; Springer: Dordrecht, The Netherlands.